PCCP

Accepted Manuscript

ROYAL SOCIETY OF CHEMISTRY

www.rsc.org/pccp

Selective Staining of Brønsted Acidity in Zeolite ZSM-5-based Catalyst Extrudates using Thiophene as a Probe

Gareth T. Whiting[1], Florian Meirer[1], Diego Valencia[1], Machteld M. Mertens[2], Anton-Jan Bons[3], Brian M. Weiss[4], Paul A. Stevens[4], Emiel de Smit[3] Bert M. Weckhuysen[1]*

[1] Inorganic Chemistry and Catalysis group, Debye Institute for Nanomaterials Science, Utrecht University, Universiteitsweg 99, 3584 CG Utrecht, The Netherlands.

[2] ExxonMobil Process Technology, ExxonMobil Research and Engineering Company, 1545 Route 22 East, Annandale, NJ 08801, United States of America.

[3] ExxonMobil Chemical Europe, Inc., European Technology Centre, Hermeslaan 2 , B-1831 Machelen, Belgium.

[4] Corporate Strategic Research, ExxonMobil Research and Engineering Company, 1545 Route 22 East Annandale, NJ 08801, United States of America.

* To whom correspondence should be addressed: B.M.Weckhuysen@uu.nl

Abstract

Optical absorption and confocal fluorescence micro-spectroscopy were applied to investigate Brønsted acidity in millimetre-sized extrudates of Na(H)-ZSM-5 and SiO_2 with varying ZSM-5 content. Partially (residual Na present) and fully proton-exchanged extrudates were employed, using thiophene oligomerization as a probe reaction. Time-resolved *in situ* optical absorption spectra and time dependent DFT calculations revealed several initial reaction pathways during the oligomerization reaction. In particular, it was found that protonated thiophene monomers reacted by either oligomerization (*via* reaction with un-reacted thiophene monomers) or ring-opening, depending on the Brønsted acid site density in each sample. Moreover, fully-exchanged extrudates not only have significantly higher reactivity than partially-exchanged samples, but they also favour the formation of ring-opening products, that are not formed on the partially-exchanged samples. Confocal fluorescence microscopy was employed to visualise non-invasively in 3D, the heterogeneity and homogeneity of thiophene oligomers on partially- and fully-exchanged extrudates,

respectively. Furthermore, it was observed that extrudates with high binder content produce a higher relative amount of conjugated species, related with a higher quantity of available monomer in the binder, which is able to react further with intermediates adsorbed on active sites. Moreover, these conjugated species appear to form near the external surface of ZSM-5 crystals/agglomerates.

Introduction

Catalysts are an important class of materials, which impact everyday life and are employed in an estimated 85 % of all chemical processes.[1,2] One of the most significant catalytic materials are zeolites, applied in a range of important processes, such as crude oil refining[3,4] and bulk chemicals synthesis.[5,6] Of particular importance is their use in isomerization[7] and alkylation[8] of hydrocarbons. In these cases, the active zeolite phase can be dispersed in other component phases, such as matrices (alumina/silica) and fillers (clay). The commercial manufacture of catalyst bodies is a neglected area in academic literature, with the shaping of both active and non-active components finely tuned to the desired needs, with pellets (μm), granules (mm) and extrudates (mm) commonly employed.[9] These catalyst bodies offer a variety of advantages over conventional zeolite powders. Physical benefits such as enhanced mass or heat transfer and mechanical resistance are recognised, with each attribute owing to their use in industrial scale reactors.[10,11]

Of particular interest are zeolite-based extrudate materials, which contain a non-homogeneously dispersed quantity of zeolite phase in a binder, such as silica or alumina. Factors such as zeolite structure, agglomeration of active phase, densification of active sites and choice of binder are known to heavily impact reactivity, selectivity and stability.[12-14] Therefore, the analysis of these factors is of crucial importance to achieve increased process efficiency. However, due to the large extrudate dimensions, the field of view is significantly reduced, requiring high spatiotemporal resolution techniques. Visualization of active material in FCC particles and similar sized catalyst bodies has advanced in the past few years, with enhancements in non-invasive spatiotemporal characterization techniques now available.[10,15] These include optical, electron and X-ray based techniques, for example, UV-Visible absorption and confocal fluorescence micro-spectroscopy (CFM),[16,17] focused-ion-beam scanning electron microscopy (FIB-SEM)[18] X-ray tomography[19] and X-ray diffraction computed tomography (XRD-CT).[20] These new techniques are ideally suited to study the active catalyst phase within an extrudate.

Optical absorption spectroscopy and CFM were used previously, to study Brønsted acidity properties in large ZSM-5 crystals and FCC particles with remarkable spatiotemporal resolution.[21–24] Probe molecule reactions, such as acid catalysed styrene and thiophene oligomerization were employed to selectively stain acid sites, providing valuable information on the strength, density and chemical component distribution within such materials.[21,25–29] Optical microscopy allowed the identification of oligomer species formed on Brønsted acid sites within each material. By exciting with a laser line wavelength close to that of a specified absorption band, fluorescent oligomer species and hence Brønsted acid site distributions can be visualized in 2D/3D using CFM.

In this work, optical micro-spectroscopy and CFM, accompanied with thiophene oligomerization as the staining probe reaction, have been used to selectively study Brønsted acidity characteristics of proton-exchanged Na-ZSM-5/SiO_2 millimetre-sized catalyst extrudates. Two series of materials are studied; partially proton-exchanged (residual Na present), and secondly, fully proton-exchanged, each containing a comparable active phase content. The aim of this study is to non-invasively distinguish Brønsted acidity variations in these fully and partially proton-exchanged millimetre-sized catalyst bodies with these micro-spectroscopic techniques. The role of zeolite content, distribution, and Brønsted acid density on the reactivity and oligomer selectivity will be investigated and visualized in 3D.

Experimental

Materials

Two series of ZSM-5 containing extrudates were prepared according to patent US6,039,864.[30] ZSM-5 crystals with Si/Al of 32 and an average crystal size of 3µm were used to make silica bound extrudates containing 20 and 80 wt.% of ZSM-5. After extrusion the materials were ion-exchanged with ammonia nitrate to result in partially (residual Na present) and fully proton-exchanged Na(H)-ZSM-5 catalysts after calcination (Table 1). Sample notations are as follows: X-*x*: where 'X' corresponds to 'H' or 'Na', denoting either series H (Na 'free') or series Na (residual Na), respectively; and *x* corresponds to the ZSM-5 content (wt. %). Example: Na-80 – Partially proton-exchanged extrudate with 80 wt. % ZSM-5 content.

Optical micro-spectroscopy

Optical micro-spectroscopy studies were performed in reflectance mode using an Olympus BX41M upright research microscope, equipped with a 50 × 0.5 NA objective lens. Illumination of the sample was performed with a 30W halogen lamp. The microscopy setup was equipped with a 50/50 double-viewport tube, which accommodated a CCD video camera (ColorView IIIu, Soft Imaging System GmbH) and an optical fiber mount. The microscope was connected to a CCD Visible spectrometer (AvaSpec-2048TEC, Avantes) by a 200 μm-core fiber. Optical spectroscopy measurements were performed using an open *in situ* cell (Linkam Scientific Instruments, FTIR 600) equipped with a temperature controller (Linkam Scientific Instruments TMS 94). Each extrudate sample used in the experiment were of similar dimensions (5 x 1.5 mm), with spectra collected from ~5 x 5 μm areas of each extrudate. To each untreated sample (water present), 5 μL of the desired probe molecule was impregnated at 303 K, before ramping (at 30 K min $^{-1}$) to 393 K. Optical absorption spectra were recorded every 10 s for a total of 1000 s.

Confocal fluorescence microscopy

A Nikon Eclipse 90*i* confocal microscope with a 100 x 0.73 NA dry objective was used for the fluorescence microscopy investigations in reflectance mode. Excitation light was provided by focusing four specific laser lines; 404, 488, 561 and 642 nm on the desired sample, located in an open (exposed to air) *in situ* cell (Linkam Instruments, FTIR 600). The microscope was equipped with a Nikon A1 scan head, accommodating the optics which couple fibre optics for excitation and emission light with the microscope. A spectral analyser in the Nikon A1 system was equipped with 32 photomultiplier tubes (PMTs) set to collect emission light in the three specific regions depending on the laser line chosen, with a resolution of 6 nm. *i.e.* 427 - 614 nm; 508 – 697 nm; 581 – 743 nm; 662 – 743 nm, corresponding with excitation wavelengths of 404, 488, 561 and 642 nm, respectively. 3D images were recorded at a similar focal depth in each sample using identical laser power. Prior to microscopic analysis, to each untreated sample (water present), 5 μL of the desired probe molecule was impregnated at 303 K, before ramping (at 30 K min $^{-1}$) to 393 K, held for 15 min, and cooled to 303 K.

Peak fitting and multivariate analysis

Generally, for each optical absorption data set (100 spectra), Principal Component Analysis (PCA) was used to determine the number of clusters needed to perform Non-Negative Matrix Factorization (NMF) (500,000 iterations used). The obtained Eigen Spectra were fitted with the minimum number of Gaussians to achieve a good fit ($R^2 > 0.99$). These Gaussians were then used as a model to fit each spectra in the time series (Figure S1). Gaussians which were determined as the background signal were removed, leaving free standing Gaussians, which provided filtered time-evolved optical absorption spectra.

Computational details

The acid catalysed formation of thiophene oligomers was elucidated for the two distinct routes depicted in Scheme 1. The ground state structures of thiophene and its condensed derivatives were obtained by means of Density Functional Theory (DFT) calculations. The optimized geometry for each compound was obtained using the hybrid meta GGA density functional M06-2X[31] with the 6-31+G(d,p) standard basis set. All harmonic vibrational frequencies were real; therefore the structures were minima on the potential energy surface.

Time dependent (TD)-DFT excited states calculations of singlet-singlet transitions were carried out at M06-2X/6-31+G(d,p) level. The M06-2X functional was selected because it had a superior performance to model the UV-Visible spectra of condensed and delocalized systems.[32,33] Ground state geometries were employed throughout all excited state calculations. Thus, the theoretical excitation energies correspond to vertical transitions which can be approximately identified as band maxima in experimental absorption spectra. All the calculations were performed with the Gaussian 09 software.[34]

Table 1: Physicochemical properties of fully and partially proton-exchanged ZSM-5 containing SiO_2 based extrudates.

Sample	ZSM-5:SiO_2 (wt. %)	Na/Al ratio	BET surface area ($m^2 g^{-1}$)	t-plot micropore area ($m^2 g^{-1}$)	Pore volume ($cm^3 g^{-1}$)	t-plot micropore volume ($cm^3 g^{-1}$)
Na-100	100:0	0.74	356	261	0.21	0.13
H-100	100:0	0.004	379	250	0.22	0.12
Na-80	80:20	0.81	353	221	0.32	0.11
H-80	80:20	0.004	366	211	0.38	0.10
Na-20	20:80	0.74	258	66	0.61	0.03
H-20	20:80	0.031	278	67	0.80	0.03
Blank	0:100	-	255	11	1.06	0

Results and discussion

Calculation of UV-Visible absorption bands in thiophene oligomers by Density Functional Theory

To obtain insight into the density of Brønsted acid sites within both partially and fully proton-exchanged series of ZSM-5-containing extrudates, the acid-catalysed oligomerization of thiophene was monitored for each sample using *in situ* optical micro-spectroscopy. Formation of oligomer species are known to be light absorbing (π-π* transitions) in the temperature ranges 333-493 K, producing specific absorption bands in the UV-Visible spectrum.[16,22] However, due to the complex intra- and inter-hydrogen transfer processes occurring, carbocation species and their specific band assignments are unclear. Therefore, Time Dependent-Density Functional Theory (TD-DFT) calculations were performed to identify the UV-Visible absorption bands of protonated thiophene oligomers.

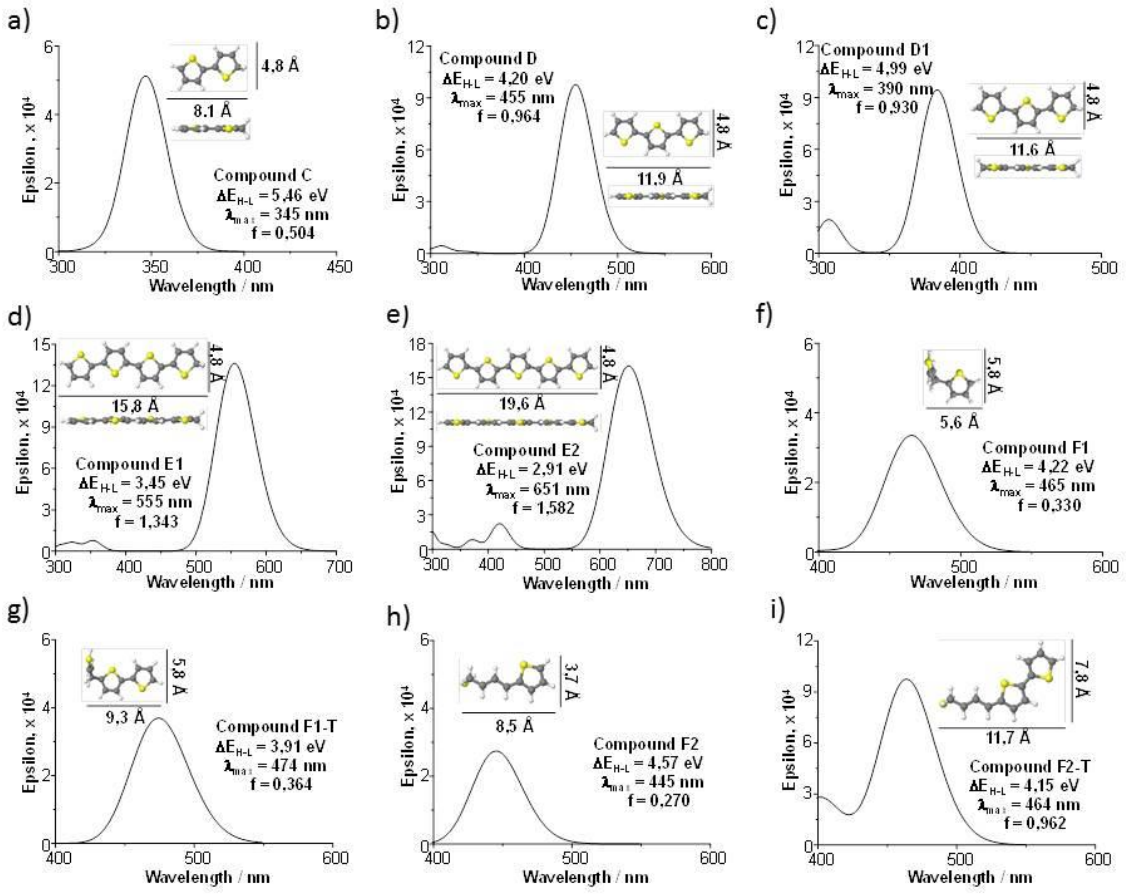

Fig. 1: Optimized geometries, molecular size, HOMO-LUMO gap (ΔE_{H-L}), wavelength of the π-π^* electronic transition (λ_{max}), oscillator strength (f) and simulated absorption spectra for the compounds in the oligomerization (a-e) and ring-opening (f-i) routes of thiophene at

M06-2X/6-31+G(d,p) level. The oligomerization products exhibited planar structures, with the trend in the ΔE_{H-L} and the λ_{max} indicating that delocalization of electrons takes place in the complete system, forming more conjugated species. The ring-opening mechanism formed two different thiol-like carbocationic species and their geometry is related to each position. Carbocation in F2 derivatives are in resonance with the thiophene ring, with the alkyl chain in the same plane. Whereas the alkyl chain in F1 derivatives is perpendicular to the aromatic ring.

Absorption bands were calculated for the main species (Fig. 1, Fig. S2, Scheme 1) identified in recent literature studies.[22,35-40] These species comprised oligomers of thiophene (C, D, E1, E2) and ring-opened thiophene (F1, F1-T, F2, F2-T). The absorption bands increased monotonically in wavelength among protonated thiophene oligomers from 276 nm for monomers to 651 nm for pentamers. The oligomers of ring-opened thiophenes had absorption bands in a narrow range between 445-474 nm. Contradictions between our TD-DFT calculations of band assignments and literature assignments do exist however, such as the trimeric carbocationic species (**D**) band position. Geobaldo *et al.* refers to this species at 416 nm when recording the UV-Vis absorption spectra of terthiophene adsorbed on zeolite H-Y.[35] However, TD-DFT calculated UV-Vis absorption spectra of the non-confined trimeric carbocation presents a band at 455 nm (Fig. 1b). This is of course a guideline, as absorption bands can shift when molecules are confined within the zeolite pore system. It is also possible that this band assignment could be due to an intermediate dimeric and/or trimeric carbocationic species, for example, a dicationic species (Fig. 1c), or as Enezel *et al*. suggests, a bithiophene radical cation, $2^{\bullet+}$, (408 nm) in acidic zeolites.[41]

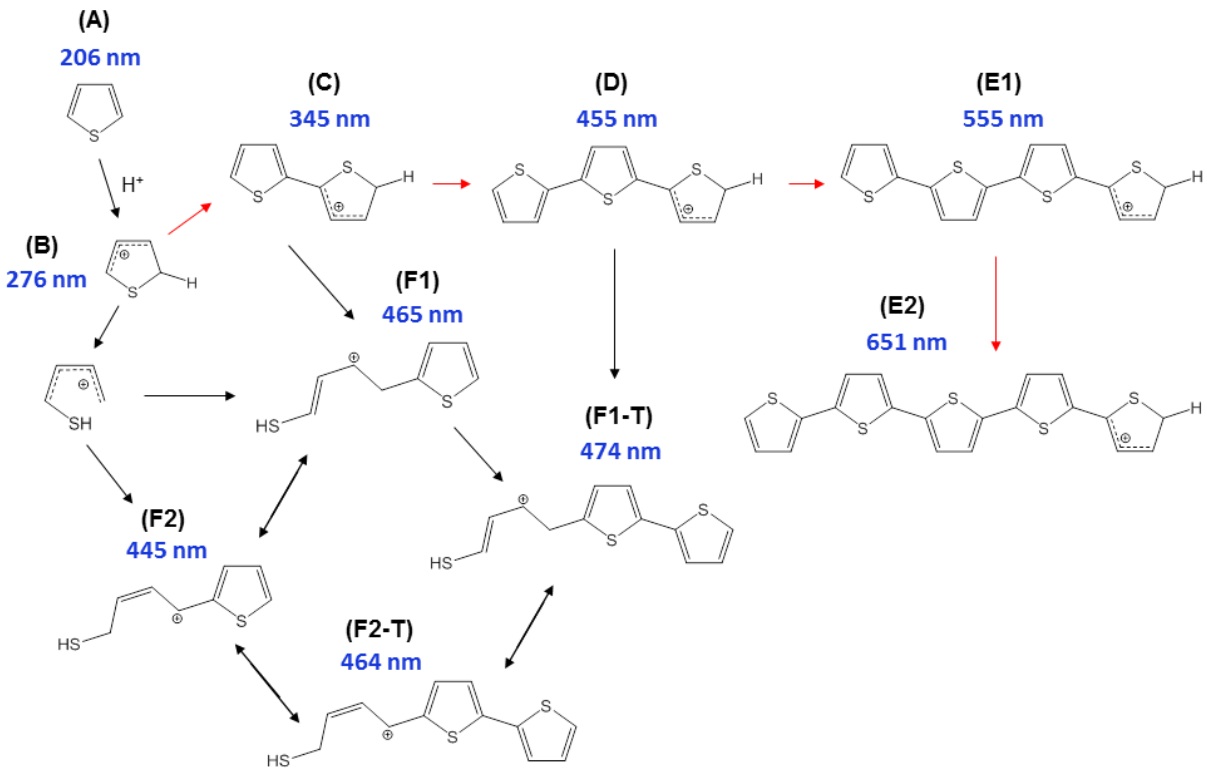

Scheme 1: Proposed reaction pathway of thiophene oligomerization on zeolite acid sites. Thiophene oligomers (**A**) undergo protonation on Brønsted acid sites of H-ZSM-5 crystals (**B**). Two different reaction pathways are possible at this stage: opening of thiophene rings and subsequent reaction with a second monomer, forming a thiol-like carbocation (**F1/F1-T/F2/F2-T**). Or, dimerization (**C**) followed by further oligomerization (**D**) or opening of the thiophene ring, forming a thiol-like carbocation (**F1/F1-T/F2/F2-T**). The trimeric carbocationic species (**D**) can undergo further oligomerization to form more extended/conjugated species (**E1/E2**).

Optical absorption spectroscopy

Due to the complex reaction pathways involved in thiophene oligomerization (Scheme 1) and the range of oligomers produced, peak fitting of optical absorption spectra and multivariate analysis were performed. An example of such analysis is presented in Fig. 2 and Fig. S1 for Na-100. Eigen spectra (obtained using PCA combined with NMF) were fitted with the minimum number of Gaussians (Fig. S1a and S1b) to create a model, prior to its application

to each spectrum in the time series (Fig. S1c). Selectively removing the background (Fig. S1d) leaves 'free-standing' absorption bands observed in Fig. 2b.

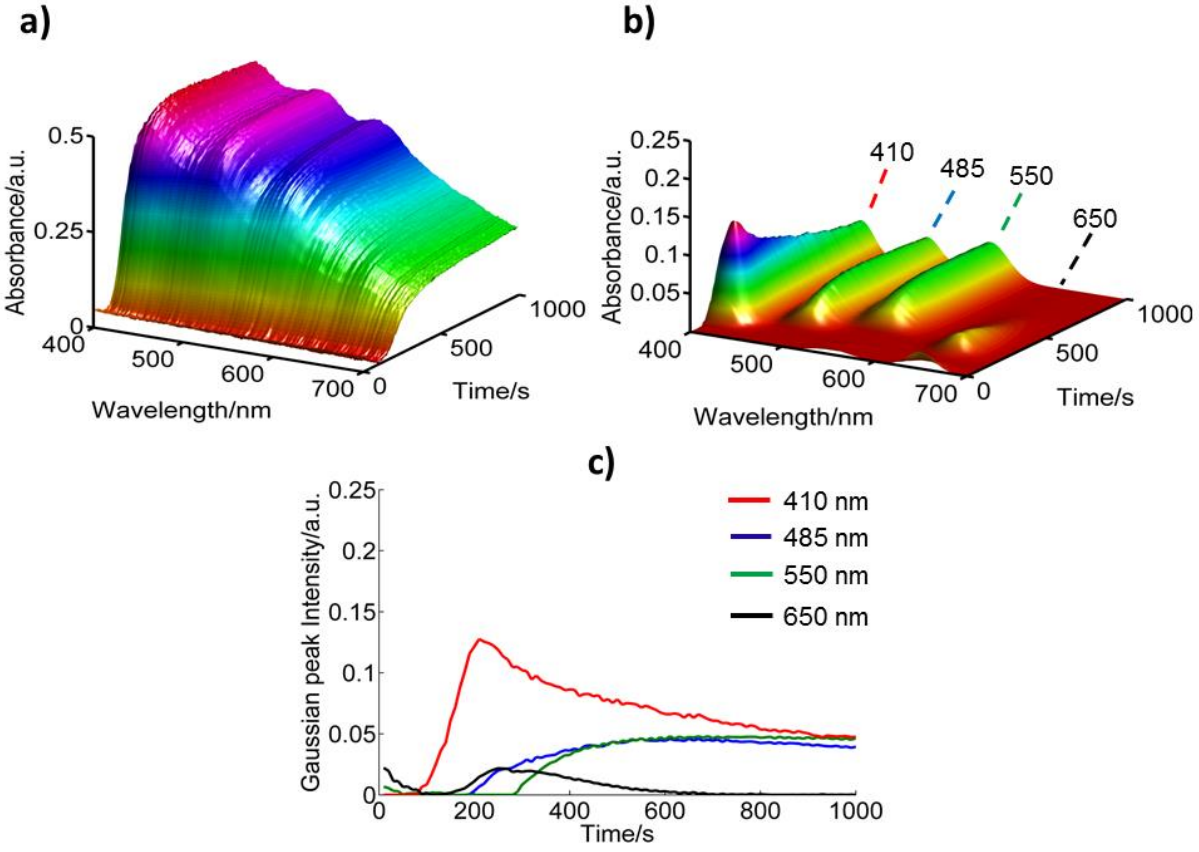

Fig. 2: a) *In situ* optical absorption spectra recorded over time during thiophene oligomerization using Na-100. Sample impregnated at 303 K before ramping (at 30 K min^{-1}) to 393 K, recording spectra every 10 s for a total of 1000 s. b) Corresponding filtered optical absorption spectra (using peak fitting and multivariate analysis), highlighting the free-standing absorption bands. c) Plot of Gaussian peak intensities used to fit each individual band displayed (top right) over the time series spectra.

The formation of four distinct absorption bands at 410, 485, 550 and 650 nm over time are presented, with the formation rate of each band displayed in Fig. 2c. The first bands to form were at 410 nm assigned to a dimeric or trimeric intermediate oligomer species, consistent with TD-DFT results. Presumably, there were other bands that formed first, representing monomers, but these bands were in the UV region, which is outside the spectral range of the instrument. A band at 650 nm, assigned to a five thiophene ring conjugated carbocation (**E2)**,

also accompanies the 410 nm band at a time of 150 s and both decrease at the same rate thereafter, suggesting they are linked in the reaction mechanism. Also evident with the decrease in formation of both the 410 and 650 nm bands, is the rise of a band at 485 nm assigned to thiol-like carbocations, **F1-T**, followed 100 s later by a band at 550 nm. According to the proposed reaction pathways in Scheme 1, the increase of the 485 nm absorption band coupled with a decrease in the 410 nm band, indicates a switch in reaction pathway, where ring opening (**F1, F1-T**)[22] of the dimer (**C**) and/or trimer (**D**) is now favoured instead of their further oligomerization. The presence of these thiol-like carbocations was also reported by Kox *et al*. using infrared spectroscopy to follow carbocations produced in H-ZSM-5 crystals reacted with 2-chlorothiophene.[42] Bands present at 2930 and 2850 cm^{-1} were attributed to aliphatic $–CH_2-$ stretching vibrations in line with those in **F** oligomer species in Scheme 1. It is indeed plausible to suggest that the exhaustion of thiophene monomers (due to the initial dimer/trimer formation) is the cause, which limits oligomerization reactions at this stage. However, the band at 550 nm has been assigned to more conjugated carbocationic species containing four thiophene units (**E1**)[35] As the band at 410 nm is assigned to either a dimeric or trimeric intermediate species, this suggests that the remaining thiophene monomers react with these adsorbed species, due to the linear increase and decrease of the 550 and 410 nm bands, respectively. Therefore, it can be stated that competing reaction pathways (ring-opening and oligomerization) are taking place at varying stages, clearly demonstrating the complexity of carbocationic assignments.

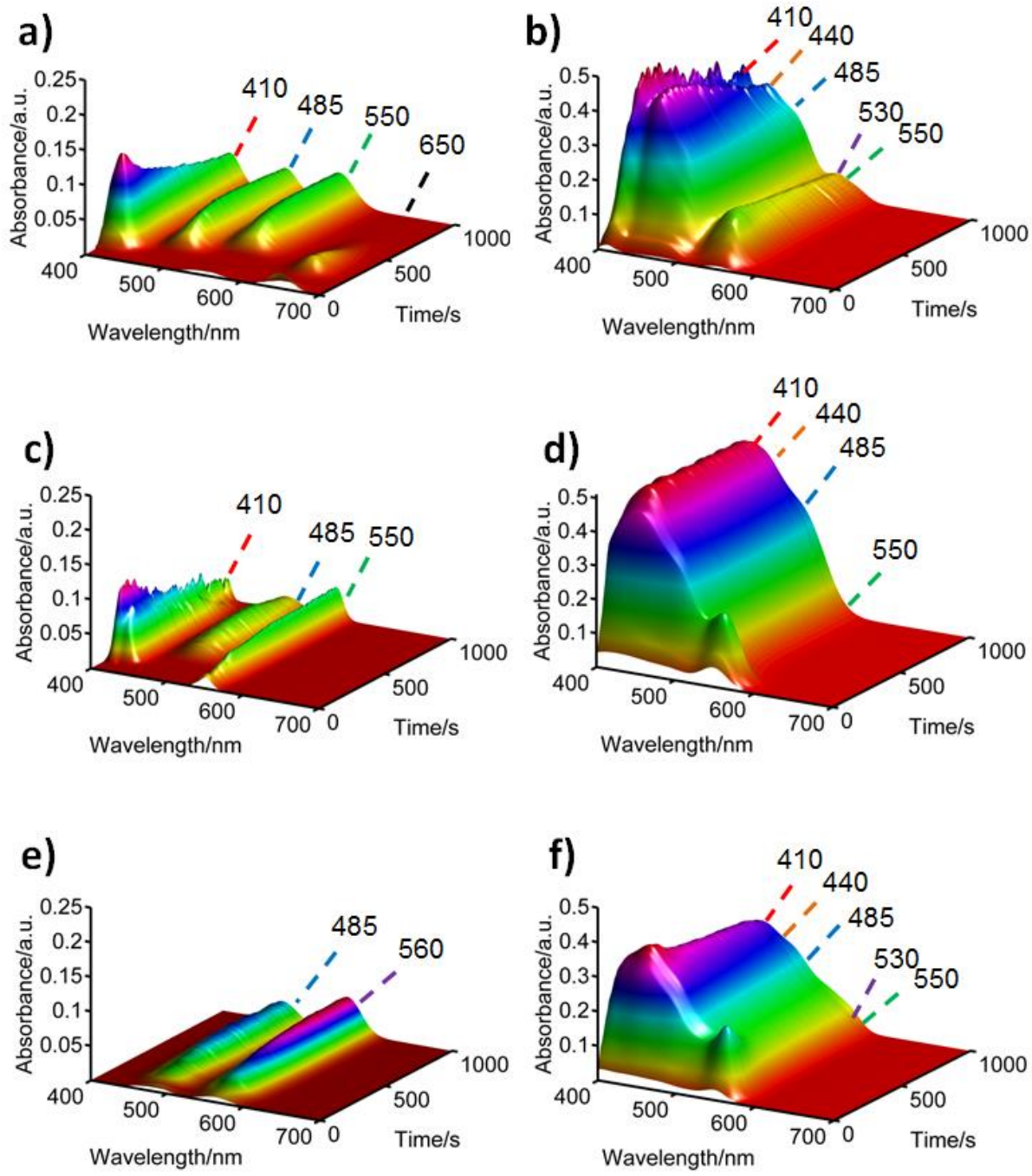

Fig. 3: Filtered *in situ* optical absorption time series spectra (using peak fitting and multivariate analysis) during thiophene oligomerization over a) Na-100 b) H-100 c) Na-80 d) H-80 e) Na-20 f) H-20. Samples impregnated at 303 K before ramping (at 30 K min $^{-1}$) to 393 K, recording spectra every 10 s for a total of 1000 s.

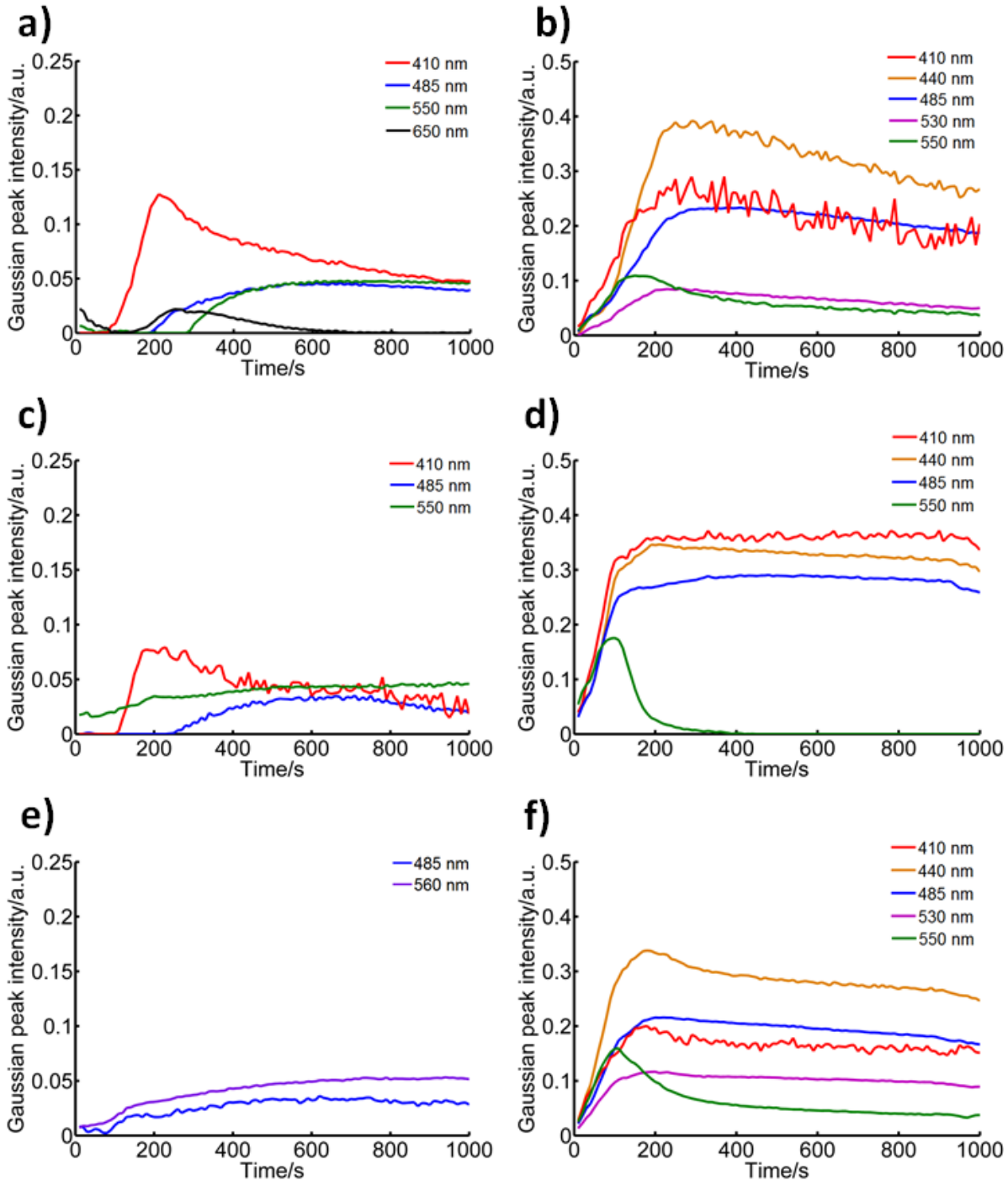

Fig. 4: Plots of Gaussian peak intensities used to fit individual absorption bands over time (related to corresponding optical absorption spectra in Fig. 2). a) Na-100 b) H-100 c) Na-80 d) H-80 e) Na-20 f) H-20.

Thiophenes reacted differently in the fully proton-exchanged H-ZSM-5 sample, as shown by the optical absorption bands in Fig. 3b. In contrast to Na-100, H-100 initially produces five

oligomer species simultaneously, but with varying rates of formation over time, observed in Fig. 4b. Accompanied by the higher overall absorbance obtained for H-100 in the raw data (Fig. S3b), in contrast to Na-100 (Fig. S3a), this clearly demonstrates the higher reactivity of fully-exchanged samples, as expected. The intense absorption band at 440 nm, not observed in Na-100, indicates that an increase in Brønsted acid site density/number plays a role in oligomer formation. Thiol-like carbocations are reported to absorb light at this wavelength (**F2**),[22] which are proposed to form from the ring opening of the initially adsorbed thiophene monomer, or *via* a ring opening of an adsorbed dimer. Also evident in Fig. 4b, is the higher rate at which the 550 nm absorption band reaches a maximum compared to other absorption bands. This is opposite to that observed with Na-100 (Fig. 4a), however, a link between the species at 550 and 440 nm is established, observing a substantial increase in absorbance of the latter band, related with a decrease in the former. Considering the low ratio of monomer to Brønsted acid sites in H-100, ring opening of monomers and/or dimers is favoured, whereas the high ratio in Na-100 favours the formation of higher oligomers.

The incorporation of 80 wt.% ZSM-5 crystals (partially-exchanged) in a SiO_2 bound extrudate (Na-80), produces a similar optical absorption spectra (Fig. 3c) to that of Na-100 during thiophene oligomerization. A significant difference within the two time series however, is the substantially increased rate of formation of the 550 nm absorption band. Although there is a lower ZSM-5 crystal content in Na-80 than in Na-100, the initial formation of more conjugated species in pure Na-ZSM-5 suggests that the SiO_2 binder is influencing reactivity. The absorption band at 550 nm is associated with a four thiophene ring carbocation (**E1**), therefore requiring a high number of unreacted thiophene monomers, and intermediate carbocations to form this species. Hence, it can be postulated that the binder stores and enhances mass transport of these monomers to the limited active sites initially.

Similarities between the raw optical spectra of H-100 and H-80 can be observed in Fig. S3b and d, respectively. Upon multivariate analysis and background removal, it is clear that although matching bands are present, the rates of formation of those produced in H-80 are significantly higher (Fig. 4d). Like Na-80, this can be attributed to the increased mass transport of the SiO_2 binder, or a more homogeneous distribution of active sites throughout the sample. Unlike in H-100, there is a dramatic decrease in absorption of the 550 nm band after 100 s. However, this is related to the higher initial reactivity, leading to limited unreacted monomers available at this reaction time, favouring the ring opening pathway, hence the intense absorption band at 440 nm. Comparing H-80 with Na-80, again emphasises

the variation in oligomer selectivity due to densification/concentration of Brønsted acid sites of fully and partially proton-exchanged samples, respectively.

As expected, due to the substantially lower ZSM-5 content accompanied by the partially-exchanged active sites, Na-20 exhibits substantially lower overall absorbance in comparison to other samples (Fig. S3e). Noticeably, Na-20 does not contain an absorption band at 410 nm as in Na-100 and Na-80. The greater number of unreacted monomers (possibly stored in the binder) in relation to the limited availability of Brønsted acid sites, could increase the further oligomerization of adsorbed dimer and/or trimer intermediate species, leading to more conjugated oligomers, such as those which absorb light at 485 and 560 nm. The band at 560 nm is clearly bathochromically shifted from that observed at 550 nm in other samples, known to occur when light absorbing molecules are positioned in different chemical environments. Na-20 contains the highest binder content compared to samples Na-100 and Na-80 and it is plausible to suggest that this particular oligomer species forms near the external ZSM-5 crystal surface into the binder. Analysed in detail, the 560 nm band experiences a hypsochromic shift (towards 550nm) throughout the reaction, suggesting these oligomer molecules increasingly form in an environment similar to that of both Na-100 and Na-80.

The optical absorption spectrum of H-20 is observed in Fig. 3f, displaying an initial formation of bands positioned at 410, 440, 485, 530 and 550 nm. The rate of formation of each band is similar to that of H-100, which, considering the lower ZSM-5 quantity indicates increased storage/mass transport of un-reacted monomers, due to the SiO_2 binder content. In contrast to the corresponding Na-20 sample, H-20 obtains a high intensity absorbance band at 440 nm, and a higher overall reactivity. As expected, this is due to the higher number of Brønsted acid sites available and the greater Brønsted acid density present.

Confocal fluorescence microscopy

Detailed 3D insight into the oligomer species spatial distribution in each series of samples was revealed using confocal fluorescence microscopy. The CFM technique employed here (Fig. 5), works by illuminating the thiophene reacted material with a specific laser line wavelength, close to the absorption band under investigation, causing the oligomer molecules (which absorb light in this region) to emit light at a higher wavelength. The focused fluorescence light is collected using a pinhole onto a detector (to view a single plane), which, after scanning varying planes with respect to the z-axis, enables a 3D image to be created. Accompanied by the optical spectroscopic results, it is already understood that oligomer

species form on the Brønsted acid sites of H-ZSM-5 crystals, which therefore allows the spatial distribution of zeolite domains within the binder of the extrudate materials.

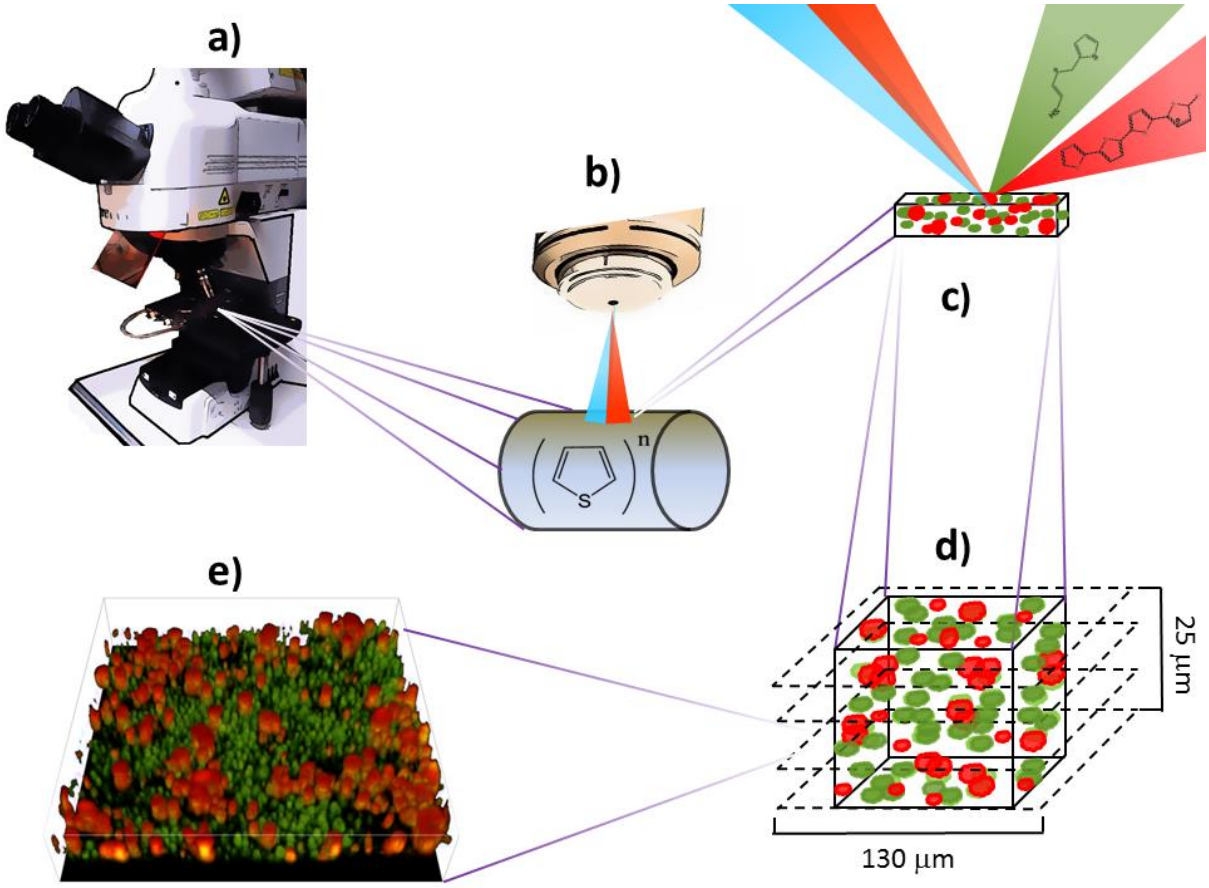

Fig. 5: Schematic of confocal fluorescence microscopy method used to record 3D fluorescence images and corresponding fluorescence spectra on zeolite-containing extrudates. a) Confocal fluorescence microscope employed to focus laser beam on the sample. Outgoing emission light is passed through a dichroic mirror and a pinhole, which selects emission light originating from a defined focal plane/depth of the sample. Finally, diffraction gratings split the emission light, which is recorded on 32 photomultiplier tubes. b) Microscopic lens used to focus incoming excitation light (of varying wavelengths) onto the reacted sample, held on a heating stage. c) Light absorbing molecules (at a specific wavelength) are excited from within the sample, emitting light at a longer wavelength (fluorescence) which is then detected d) Emission light is recorded from single planes from a set depth range within the sample, which is processed to form e) a 3D reconstruction of the scanned volume, displaying distribution of fluorescent domains.

As revealed by optical absorption spectra for Na-100 (Fig. 3a), four main absorption bands were recorded at 410, 485, 550 and 650 nm, associated with light absorbing oligomer species with increasing levels of conjugation, respectively. The oligomer species giving rise to the absorption band at 410 nm are readily excited using a 404 nm laser. (2D image shown in inset of Fig. S5a). The introduction of a dichroic mirror at 488 nm is mandatory with this particular microscopic setup, and unfortunately is centred around the main fluorescence band produced, therefore filtering out the majority of the signal.

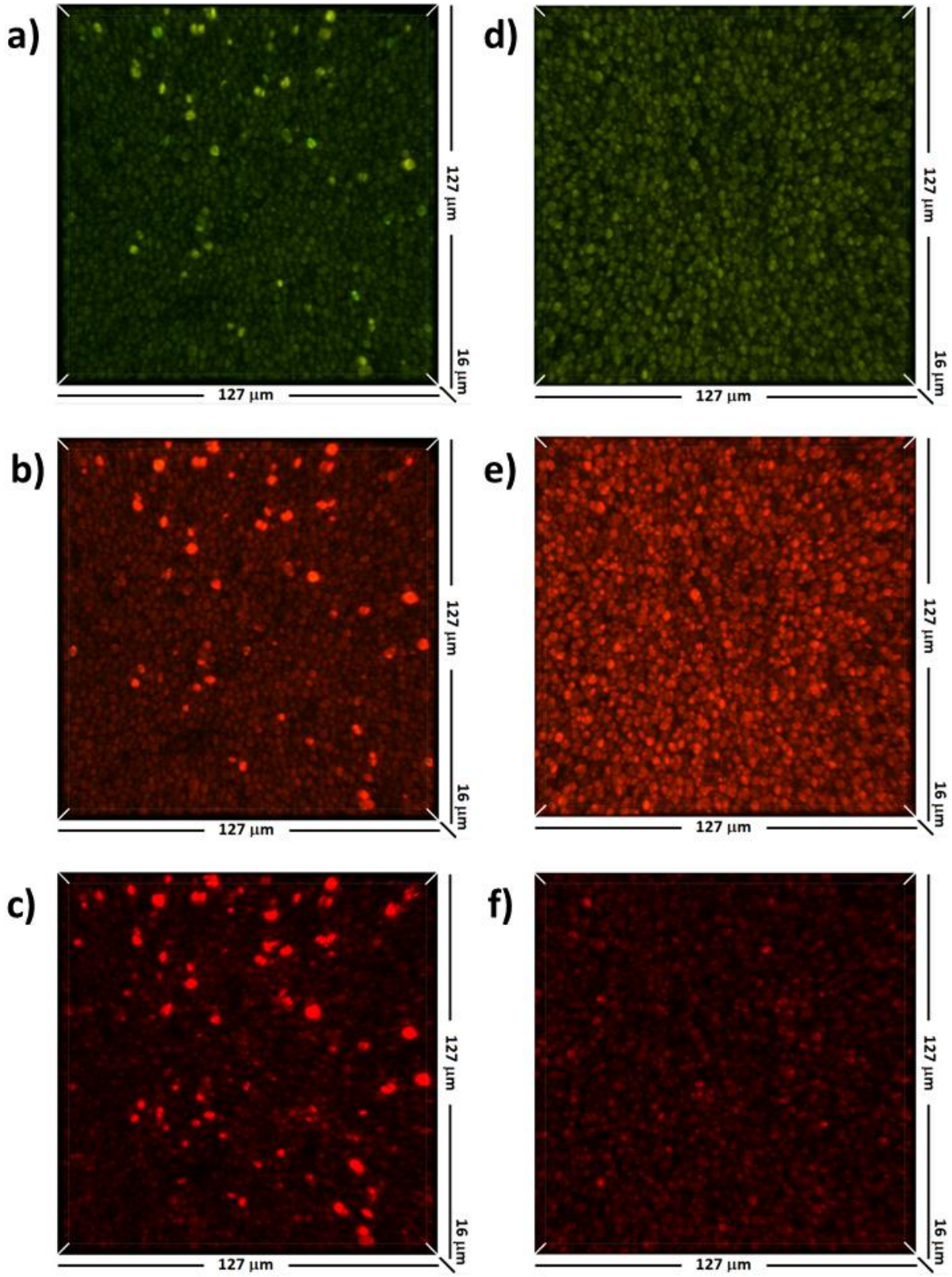

Fig. 6: Top view 3D confocal fluorescence images of Na-100 (a-c) and H-100 (d-f) after thiophene oligomerization. Excited with 488 nm laser; top panels; 561 nm laser centre panels; and 642 nm laser; bottom panels (white circles depict region of interest).

Fig. 6a displays the 3D fluorescence image produced by exciting Na-100 with a 488 nm laser. The green domains are attributed to the presence of the fluorescent thiol-like carbocationic species within H-ZSM-5 crystals/agglomerates (2-3 μm), which absorb light at 485 nm (**F1-T**). A minority of the zeolite crystals in the partially-exchanged sample fluoresced more intensely (depicted by white circles) than the majority of the crystals. This becomes more evident when exciting the more conjugated oligomers which absorb light at 550 nm, with a 561 nm laser. Fig. 6b shows that the majority of the ZSM-5 agglomerates within view are moderately fluorescent, however, the same select agglomerates excited with a 488 nm laser are again intensely fluorescent after excitation with a 561 nm laser. The lower fluorescence intensity of the partially-exchanged crystals is related to the Na/Al ratio (0.74) measured for Na-100 (Table 1). Although this material is only partially proton-exchanged, it is possible that a number of crystals/agglomerates were proton-exchanged to a further extent than the majority. Therefore, it is possible to distinguish between active agglomerates and partially/non-active crystals/agglomerates and their distribution using CFM. In order to excite more conjugated oligomer species, without the possibility of exciting less conjugated species (< 500 nm), a 642 nm laser was used (Fig. 6c). Although the fluorescent intensity decreases with the 642 nm laser (Fig. S5b), the agglomerates visible in Fig. 6a appear to increase slightly in size, which suggest that these more extended species form near the external surface of each agglomerate. This could be due to the steric hindrance of these particular oligomer species within the pores of the ZSM-5 crystals, agreeing with the molecular growth proposed,[11] owing to four or more thiophene unit containing species.

CFM measurements performed on H-100 confirms the results observed in the optical spectra (Fig. S3b). Although the fluorescence intensity obtained for H-100 (Fig. 6d) is similar to that of Na-100 when exciting with a 488 nm laser, there is a more homogeneous selectivity towards this oligomer species from each agglomerate within the field of view. Excitation of more conjugated species with a 561 nm laser (Fig. 6e) leads to intense fluorescence, which is again more homogeneously distributed, but is also higher than that observed for Na-100 (Fig. S5b). This corresponds well with the results observed in the optical microscopy experiments (Fig. S3a and b), where H-100 achieves a greater absorbance. As with that observed for Na-100, weak fluorescence is obtained for H-100 when exciting with a 642 nm laser (Fig. 6f).

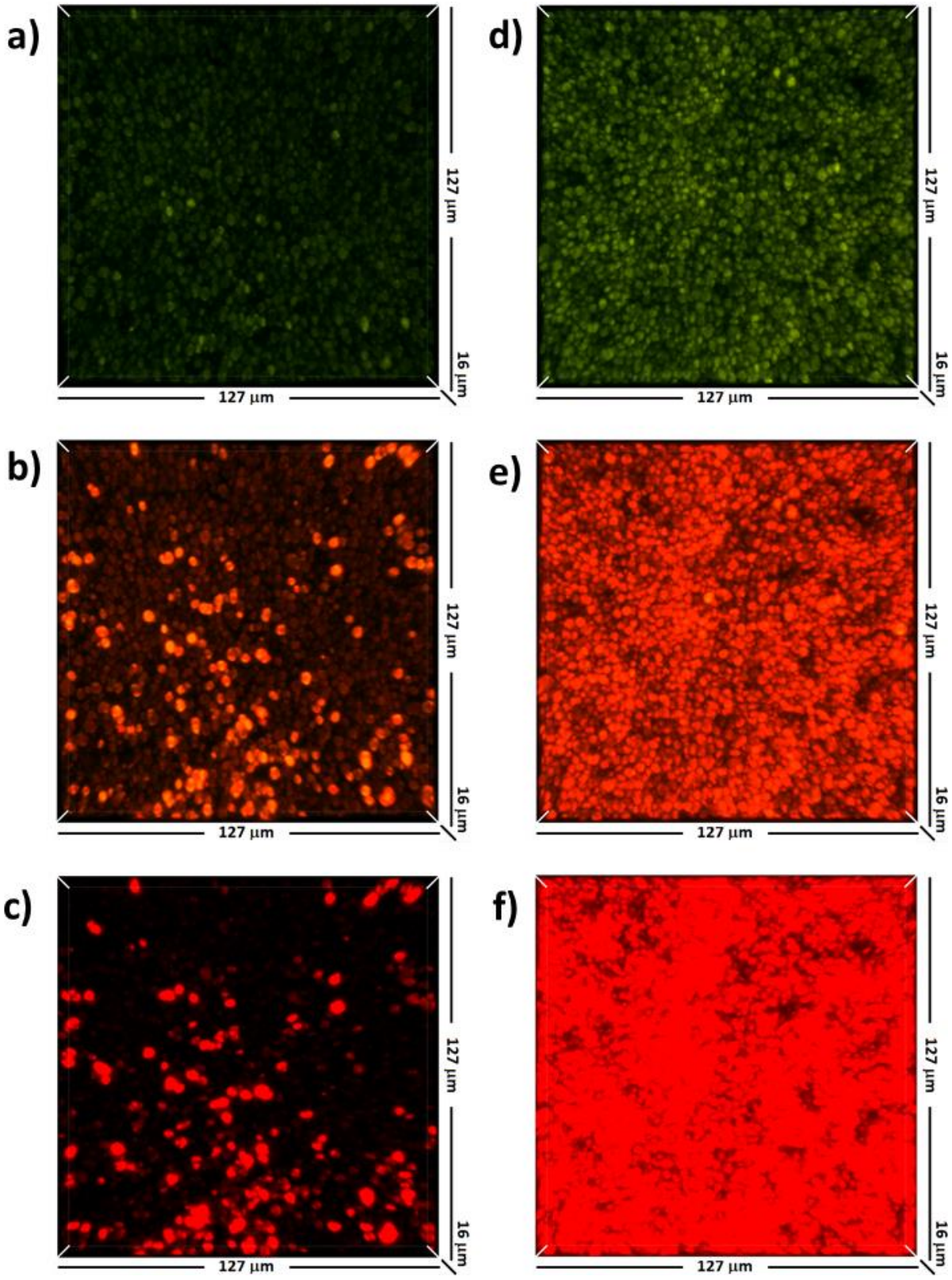

Fig. 7: Top view 3D confocal fluorescence images of Na-80 (a-c) and H-80 (d-f) after thiophene oligomerization. Excited with 488 nm laser; top panels; 561 nm laser centre panels; and 642 nm laser; bottom panels.

In order to gain insight into the ZSM-5 crystal reactivity when extruded in a binder, both series of extrudates were analysed. In association with the optical absorption spectra of both Na-80 and H-80 (Fig. S3a and b, respectively), CFM measurements using a 488 nm laser detected the same trend, whereby higher fluorescence was obtained for the fully-exchanged sample (Fig. S5c). As with Na-100, 3D CFM images of Na-80 (Fig. 7a) show that only a few agglomerates are fluorescent at this wavelength, whereas H-80 displays a more homogeneous fluorescence distribution (Fig. 7d).

With the higher quantity of Brønsted acid sites present in H-80 compared with Na-80 (Table 1), the former had a far higher reactivity, and produced a higher ratio of more conjugated species, as displayed in the optical absorption spectra (Fig. 3c and d). Excitation using a 561 nm laser clearly confirms this result, with H-80 achieving an intense fluorescence band at 613 – 666 nm when compared with Na-80 (Fig. S5c). CFM 3D images provide greater insight, showing a larger number of fluorescent agglomerates (Fig. 7e) than Na-80 (Fig. 7b). Detailed analysis of the fluorescence spectra of H-80 (Fig. S5c) reveals that two bands exist, at 613 - 672 nm and 666 – 714 nm. This indicates that excitation using a 561 nm laser probably excites two separate oligomer species. By exciting H-80 with a 642 nm laser, the fluorescence spectra shows the same band 666-714 nm is obtained as with excitation at 561 nm. Therefore it clearly distinguishes that the 561 nm laser excites both less and more conjugated oligomer species in this material simultaneously. Also noticeable in the fluorescence spectra is the substantially higher overall fluorescence intensity of H-80 compared with Na-80, which again corresponds well with the optical absorption spectra (Fig. S3c and d). Fig. 7c and f confirm these results, with H-80 revealing a far greater quantity of fluorescent H-ZSM-5 agglomerates than Na-80. As stated previously, the significantly higher absorbance >560 nm can be assigned to the higher reactivity of H-80, due to a greater quantity of Brønsted acid sites being available, leading to more conjugated oligomer formation. Exciting both materials with 488 and 642 nm lasers simultaneously reveals the extent of more conjugated species, compared with less conjugated species in H-80 in comparison to Na-80. Fig. 8a and b display the 3D CFM images for these materials. A select few agglomerates contain more extended oligomer species (orange), in contrast to the majority of crystals which contain only less conjugated species (green). H-80 reveals that the majority of agglomerates visible contain both less and more conjugated species, forming a yellow fluorescence.

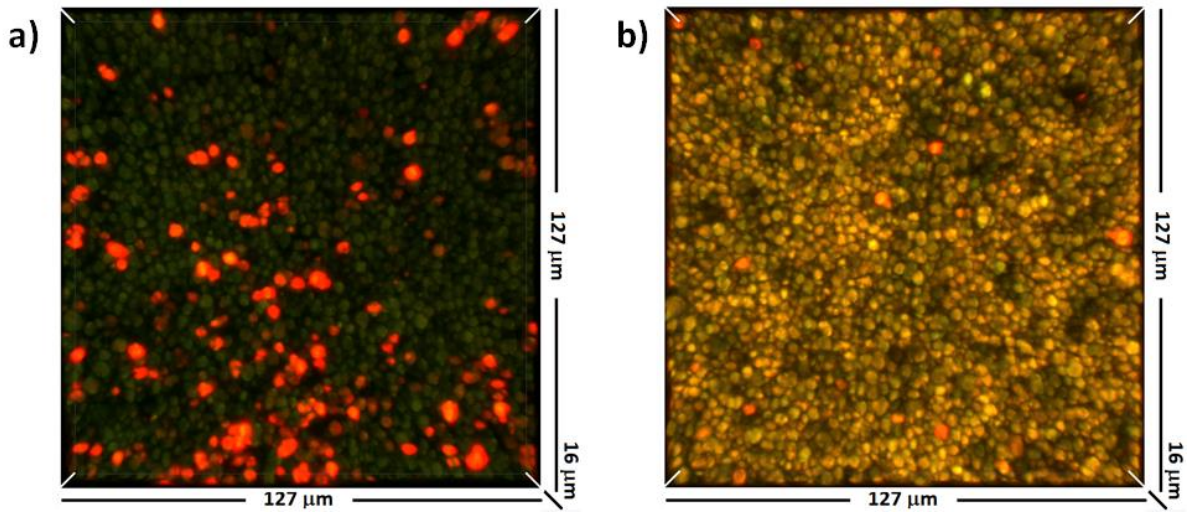

Fig. 8: Top view 3D confocal fluorescence images of Na-80 (a) and H-80 (b) after thiophene oligomerization. Excited with 488 and 642 nm lasers simultaneously.

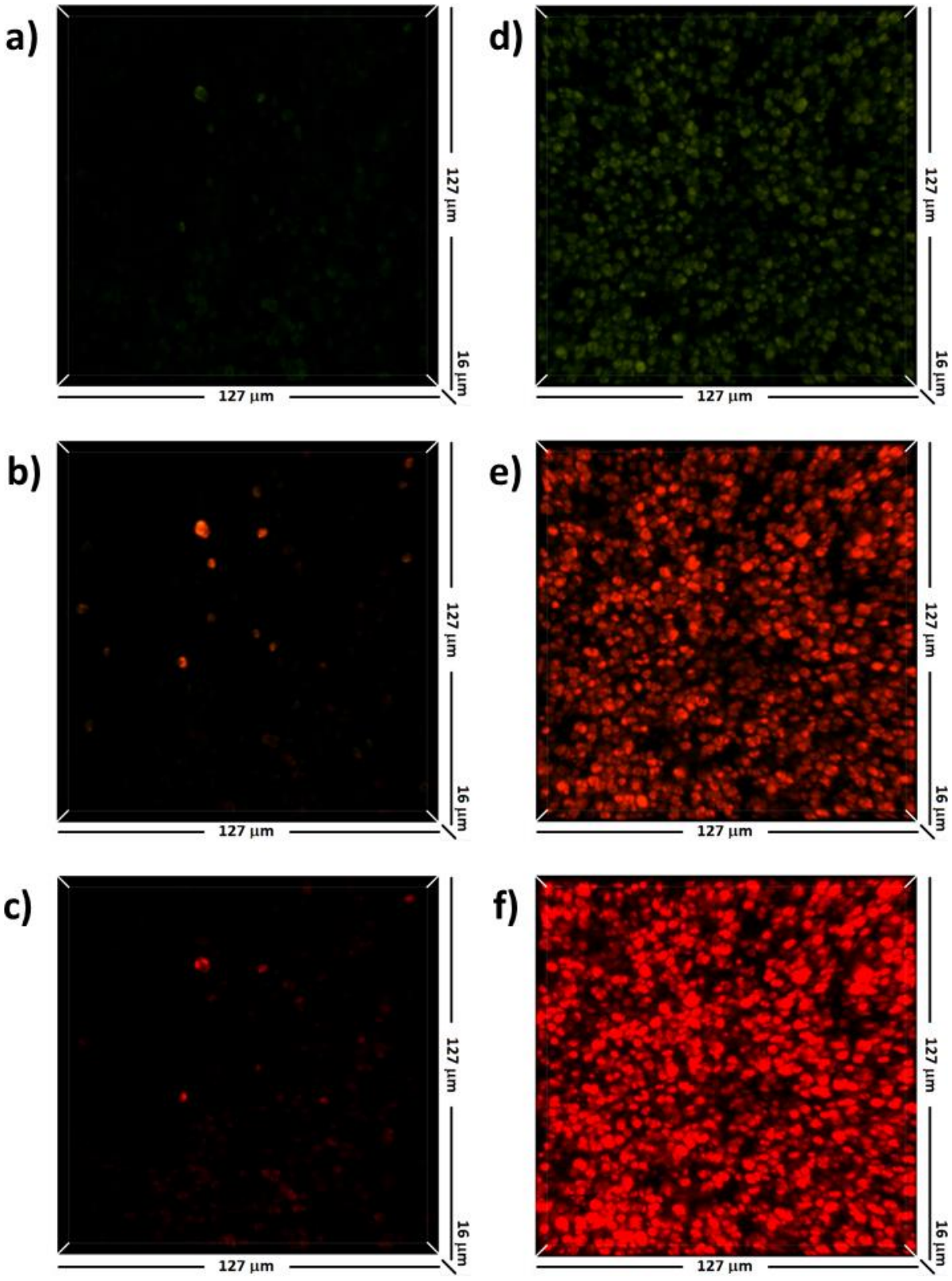

Fig. 9: Top view 3D confocal fluorescence images of Na-20 (a-c) H-20 (d-f) after thiophene oligomerization. Excited with 488 nm laser; top panel; 561 nm laser centre panel; and 642 nm laser; bottom panel.

The optical absorption spectra of both Na-20 and H-20 (Fig. 3e and f, respectively) show that not only does the quantity and density of Brønsted acid sites affect oligomer selectivity, but it is also affected by the binder content in the material. Due to the significantly lower quantity of active phase present in Na-20, its reactivity is correspondingly far lower than that of Na-80. This becomes apparent when measuring the fluorescence of Na-20 (Fig. S5d). CFM 3D images are shown in Fig. 9a-c. As expected, only a few agglomerates are weakly fluorescent when exciting separately with 488, 561, and 642 nm laser lines. H-20, however, achieves a far more homogeneous fluorescence over the area shown (Fig. 9d-f), again, corresponding well with optical absorption results displayed in Fig. 3f. From both series of materials, it becomes clear that with increasing binder concentration follows an affinity for more conjugated species, in comparison to less conjugated species. Although many binder effects have been proposed in the literature, it is not easy to state with certainty those taking place during the oligomerization of thiophene in these materials. Given the increased tendency to form more conjugated species, it suggests that the binder stores thiophene monomers, which are transported to react further with intermediate carbocations adsorbed on H-ZSM-5 crystals.

Conclusions

A combination of optical and confocal fluorescence micro-spectroscopy has been used to study the location and nature of thiophene carbocations originating from Brønsted acid sites in ZSM-5-containing extrudates. Thiophene oligomerization was performed on two series of Na(H)-ZSM-5 containing SiO_2 bound extrudates. Firstly, partially proton-exchanged (residual Na present) and secondly, fully proton-exchanged, both containing 100, 80 and 20 wt. % active content. The fully-exchanged series of extrudates achieved substantially higher reactivity, revealing that quantity of the Brønsted acid sites is an overriding factor for this reaction. It was found using time-resolved optical spectroscopy and TD-DFT calculations that a number of reaction pathways develop over time, which are dependent on the Brønsted acid site density and quantity. In general, a decrease in H-ZSM-5 content in the extrudate favours the formation of more conjugated species, related to the higher binder content present and hence, the higher quantity of monomers stored to react further *per* active site. The higher Brønsted acid site density present in fully-exchanged extrudates led to the formation of thiol-like carbocations *via* a ring-opening mechanism, not favoured in partially-exchanged samples due to the isolation of Brønsted acid sites. Correlating optical absorption findings with confocal fluorescence microscopy allowed the visualization of these aspects non-invasively in 3D. Selectively exciting less/more conjugated carbocations created Brønsted acidity maps,

where larger conjugated species appeared to extend from the external surface of individual crystals/agglomerates.

Acknowledgements

This work is supported by ExxonMobil and an European Research Council (ERC) Advanced Grant (no. 321140).

References

1. P. T. Anastas, M. M. Kirchhoff, and T. C. Williamson, *Appl. Catal. A Gen*., 2001, **221**, 3–13.
2. W. F. Hölderich, J. Röseler, G. Heitmann, and A. T. Liebens, *Catal. Today*, 1997, **37**, 353–366.
3. A. Corma, M. J. Díaz-Cabañas, J. Martínez-Triguero, F. Rey, and J. Rius, *Nature*, 2002, **418**, 514–517.
4. W. Vermeiren and J.-P. Gilson, *Top. Catal.*, 2009, **52**, 1131–1161.
5. A. Corma, *Chem. Rev.*, 1995, **95**, 559-614
6. M. J. Climent, A. Corma, and S. Iborra, *Chem. Rev*., 2011, **111**, 1072–1133.
7. A. de Lucas, J. L. Valverde, P. Sánchez, F. Dorado and M. J. Ramos, *Ind. Eng. Chem. Res*., 2004, **43**, 8217–8225.
8. C. Perego and P. Ingallina, *Catal. Today*, 2002, **73**, 3-22.
9. S. Mitchell, N.-L. Michels, K. Kunze, and J. Pérez-Ramírez, *Nat. Chem*., 2012, **4**, 825–831.
10. S. Mitchell, N.-L. Michels, and J. Pérez-Ramírez, *Chem. Soc. Rev*., 2013, **42**, 6094–6112.
11. J. S. J. Hargreaves and A. L. Munnoch, *Catal. Sci. Technol*., 2013, **3**, 1165-1171
12. P. Castaño, J. Ruiz-Martínez, E. Epelde, A. G. Gayubo, and B. M. Weckhuysen, *ChemCatChem*, 2013, **5**, 2827–2831.
13. A. de Lucas, J. L. Valverde, P. Sánchez, F. Dorado, and M. J. Ramos, *Ind. Eng. Chem. Res*., 2004, **43**, 8217–8225.
14. P. Cañizares, A. Durán, F. Dorado, and M. Carmona, *Appl. Clay Sci*., 2000, **16**, 273–287.
15. I. L. C. Buurmans, J. Ruiz-Martínez, W. V Knowles, D. van der Beek, J. A. Bergwerff, E. T. C. Vogt, and B. M. Weckhuysen, *Nat. Chem*., 2011, **3**, 862–867.

16. J. Ruiz-Martínez, I. L. C. Buurmans, W. V. Knowles, D. van der Beek, J. A. Bergwerff, E. T. C. Vogt, and B. M. Weckhuysen, *Appl. Catal. A Gen.*, 2012, **419-420**, 84–94.
17. L. Karwacki and B. M. Weckhuysen, *Phys. Chem. Chem. Phys.*, 2011, **13**, 3681–5.
18. L. Karwacki, D. A. M. de Winter, L. R. Aramburo, M. N. Lebbink, J. A. Post, M. R. Drury, and B. M. Weckhuysen, *Angew. Chem. Int. Ed.*, 2011, **50**, 1294–1298.
19. J.-D. Grunwaldt and C. G. Schroer, *Chem. Soc. Rev.*, 2010, **39**, 4741–4753.
20. J. Ruiz-Martínez, A. M. Beale, U. Deka, M. G. O'Brien, P. D. Quinn, J. F. W. Mosselmans, and B. M. Weckhuysen, *Angew. Chem. Int. Ed.*, 2013, **52**, 5983–5987.
21. L. R. Aramburo, J. Ruiz-Martínez, J. P. Hofmann, and B. M. Weckhuysen, *Catal. Sci. Technol.*, 2013, **3**, 1208-1214.
22. M. H. F. Kox, A. Mijovilovich, J. J. H. B. Sättler, E. Stavitski, and B. M. Weckhuysen, *ChemCatChem*, 2010, **2**, 564–571.
23. I. L. C. Buurmans, E. A. Pidko, J. M. de Groot, E. Stavitski, R. A. van Santen, and B. M. Weckhuysen, *Phys. Chem. Chem. Phys.*, 2010, **12**, 7032–7040.
24. I. L. C. Buurmans and B. M. Weckhuysen, *Nat. Chem.*, 2012, **4**, 873–886.
25. M. M. Kerssens, C. Sprung, G. T. Whiting, and B. M. Weckhuysen, *Micropor. Mesopor. Mat.*, 2014, **189**, 136-143.
26. G. De Cremer, B. F. Sels, D. E. De Vos, J. Hofkens, and M. B. J. Roeffaers, *Chem. Soc. Rev.*, 2010, **39**, 4703–4717.
27. P. Chen, X. Zhou, H. Shen, N. M. Andoy, E. Choudhary, K.-S. Han, G. Liu, and W. Meng, *Chem. Soc. Rev.*, 2010, **39**, 4560–4570.
28. M. B. J. Roeffaers, R. Ameloot, M. Baruah, H. Uji-i, M. Bulut, G. de Cremer, U. Müller, P. A. Jacobs, J. Hofkens, B. F. Sels, D. E. de Vos, *J. Am. Chem. Soc.*, 2008, **130**, 5763–5772.
29. M. B. J. Roeffaers, B. F. Sels, H. Uji-i, B. Blanpain, P. L'hoëst, P. A. Jacobs, F. C. De Schryver, J. Hofkens, and D. E. De Vos, *Angew. Chem. Int. Ed.*, 2007, **46**, 1706–1709.
30. G. D. Mohr, J. P. Verduijn (Exxon Chemical Patents Inc.), US6039864, 2000.
31. Y. Zhao and D. G. Truhlar, *Theor. Chem. Acc.*, 2007, **120**, 215–241.
32. A. Charaf-Eddin, A. Planchat, B. Mennucci, C. Adamo, and D. Jacquemin, *J. Chem. Theory Comput.*, 2013, **9**, 2749–2760.
33. D. Jacquemin, Y. Zhao, R. Valero, C. Adamo, I. Ciofini, and D. G. Truhlar, *J. Chem. Theory Comput.*, 2012, **8**, 1255–1259.

34. Gaussian 09. Revision B.01, M. J. Frisch, *et al*. (Gaussian, Inc., Wallingford CT, 2009). See the Supporting Information, S6.
35. F. Geobaldo, T. Palomino, S. Bordiga, C. Fisica, A. Zecchina, and C. O. Areán, *Phys. Chem. Chem. Phys*.,1999, **1**, 561–569.
36. A. Corma and H. García, *J. Chem. Soc. Dalton Trans*., 2000, 1381–1394.
37. H. H. Shan, C. Y. Li, C. H. Yang, H. Zhao, B. Y. Zhao, and J. F. Zhang, *Catal. Today*, 2002, **77**, 117–126.
38. L. Jaimes, M. L. Ferreira, and H. de Lasa, *Chem. Eng. Sci*., 2009, **64**, 2539–2561.
39. S. Y. Yu, J. Garcia-Martinez, W. Li, G. D. Meitzner, and E. Iglesia, *Phys. Chem. Chem. Phys*., 2002, **4**, 1241–1251.
40. A. Chica, K. Strohmaier, and E. Iglesia, *Langmuir*, 2004, **20**, 10982–10991.
41. P. Enzel and T. Bein, *Synth. Met*., 1993, **55**, 1238–1245.
42. M. H. F. Kox, K. F. Domke, J. P. R. Day, G. Rago, E. Stavitski, M. Bonn, and B. M. Weckhuysen, *Angew. Chem. Int. Ed*., 2009, **48**, 8990–8994.